Molecular orientational structure of the water liquid/vapour interface

1991 J. Phys.: Condens. Matter 3 F109

(http://iopscience.iop.org/0953-8984/3/42/010)

J. Phys.: Condens. Matter 3 (1991) F109–F125. Printed in the UK

Molecular orientational structure of the water liquid/vapour interface

B Yang, D E Sullivan, B Tjipto-Margo† and C G Gray
Physics Department and Guelph-Waterloo Program for Graduate Work in Physics, University of Guelph, Guelph, Ontario N1G 2W1, Canada

Received 20 May 1991

Abstract. Theoretical and experimental results for the distribution of molecular orientations at the liquid/vapour interface of water are compared. The present calculations are based on an extended mean-field density functional theory applied to an intermolecular potential model containing dipolar and quadrupolar interactions, with parameters chosen to agree with the TIP4P model of water. The results for the orientational order parameters at the interface are used to calculate several observable quantities as functions of temperature, namely: (i) the surface electrostatic potential; (ii) the coefficient of ellipticity; (iii) the nonlinear susceptibility measured by second-harmonic generation. Comparisons are made with both the experimental and computer simulation data for water. The limitations of current methods for revealing the preferred molecular orientations at an interface are discussed.

1. Introduction

Recently, using the x-ray reflectivity technique [1], there has been progress in the long-standing problem [2] of the experimental determination of the number density profile $\rho(z)$ at the liquid/vapour interface. For molecular fluids such as N_2, HCl and H_2O, the more detailed quantity $\rho(z, \omega)$ is also of interest, giving the distribution of density and molecular orientation ω along the direction z normal to the surface. In this paper we briefly review some relevant experiments, and compare the results of our recent extended mean-field-theory calculations for water [3] with experiment, and also with the results from computer simulations [4, 5].

Previous theoretical [6–11] and simulation work [12, 13] for $\rho(z, \omega)$ has been limited to linear molecules, apart from the recent simulations of water [4, 5, 14, 15] and methanol [16]. In comparing our calculations with simulations we mainly restrict ourselves to [4, 5], since the potential model (TIP4P) employed is closest to the one we use (see section 4).

It has been found necessary [3, 11] to extend the standard mean-field theory by including pair correlations to the lowest order contributing, in order to obtain orientational symmetry breaking in the interfacial region. We also find it necessary to include quadrupolar, as well as dipolar, intermolecular forces, in order to break the xy-plane

† Present address: Department of Chemistry, Oregon State University, Corvallis, OR 97331, USA.

0953-8984/91/42F109 + 17 $03.50

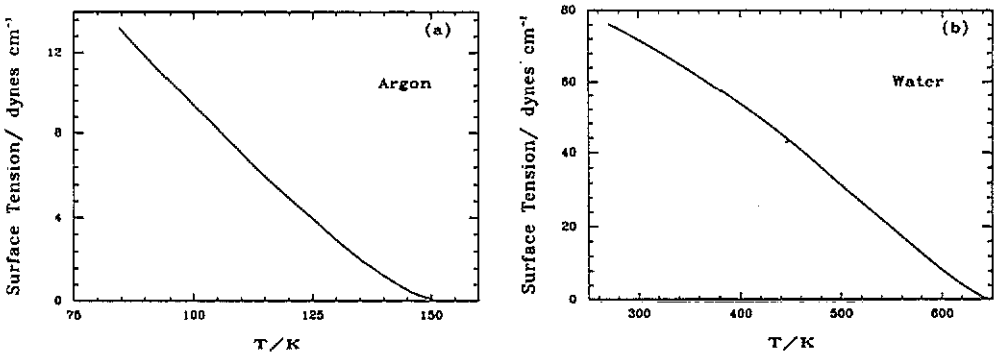

Figure 1. The surface tension of (*a*) Ar (from [17]) and (*b*) H_2O (from [18]) as a function of temperature.

reflection symmetry. We find a slight preference for the water dipole molecules at the interface to be pointing downwards (i.e. towards the liquid side) compared with upwards.

2. Review of relevant experiments

2.1. Surface entropy

We recall the relation [2] $S^s = -d\gamma(T)/dT$ between the surface entropy S^s and surface tension $\gamma(T)$, where T is the temperature. In figure 1 we show $\gamma(T)$ for Ar and H_2O. Note that $|d\gamma(T)/dT|$ increases monotonically for Ar with decreasing T, whereas there is an inflection point for H_2O at $T \simeq 525$ K. We interpret the decreasing slope below 525 K for H_2O as evidence of interfacial orientational ordering, which reduces the surface entropy. The evidence is obviously indirect, and it is impossible to obtain details of the preferred molecular orientations from surface entropy measurements.

2.2. Surface potential

The surface potential $\Delta\varphi$ is the work done per unit charge in moving a hypothetical test charge through the interface, from the vapour to the liquid side. For non-polarizable molecules $\Delta\varphi$ is given rigorously by [19]

$$\Delta\varphi = -4\pi\mu \int_{-\infty}^{\infty} dz\, \rho(z)\langle\cos\theta\rangle - 2\pi\Theta(\rho_L - \rho_G) \tag{2.1}$$

where θ is the angle between the molecular dipole moment $\boldsymbol{\mu}$ and the z-axis, where positive z corresponds to the vapour side of the interface,

$$\langle \ldots \rangle = \int d\omega \hat{f}(z, \omega)(\ldots)$$

with $\hat{f}(z, \omega)$ the orientational distribution function defined in (3.5) below, ρ_L and ρ_G are the bulk liquid and vapour densities, respectively, and $\Theta = \frac{1}{3}\Sigma_i q_i r_i^2$ is one third of the trace of the quadrupole moment tensor of an isolated molecule (see, e.g., equation (2.54) of [20]). The derivation of (2.1) is discussed further in section 4.3.

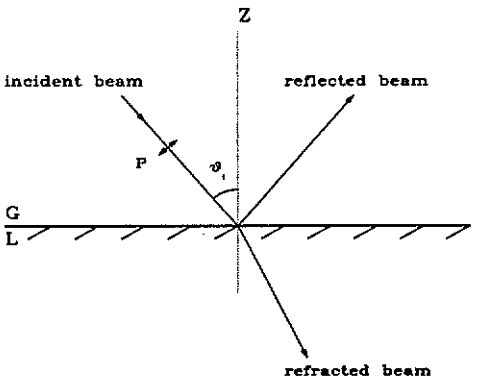

Figure 2. A schematic diagram of an ellipsometry experiment, with the polarization vector $\boldsymbol{p}$ in the plane of the page. G and L denote the gas and liquid sides of the interface, respectively.

Since experiments are performed using real ions that interact with water molecules (e.g., solvation occurs), rather than with hypothetical test charges, the relation between (2.1) and what is measured is somewhat obscure [5]. For water, $\Delta\varphi$ appears to be positive, and about 50 mV in magnitude [5]. As we shall see, the quadrupole term appears to be much larger than the dipole term for water, which precludes learning much about $\langle\cos\theta\rangle$ for water from $\Delta\varphi$ measurements.

2.3. Ellipsometry

In figure 2 we show schematically a beam of light partially reflected off the liquid surface, with polarization state $\boldsymbol{p}$ of the incident beam in the scattering plane as shown. If the angle of incidence θ_i equals the Brewster angle θ_B, the reflected intensity vanishes, by the definition of θ_B. In actuality, the reflected intensity completely vanishes only for an infinitely sharp interface. The real interface is at least a few angstroms thick, and the reflected amplitude is proportional to $\eta = \eta_0 + \Delta\eta$, where the isotropic and anisotropic contributions are given by (see section 4.4)

$$\eta_0 = \int_{-\infty}^{\infty} dz\,[\varepsilon(z) - \varepsilon^L][\varepsilon(z) - \varepsilon^G]/\varepsilon(z) \tag{2.2}$$

$$\Delta\eta = -\tfrac{1}{6}\int_{-\infty}^{\infty} dz\,[\varepsilon(z) - 1][\varepsilon(z) + 2]\left(1 + 2\frac{\varepsilon^L\varepsilon^G}{\varepsilon(z)^2}\right)\frac{\overline{\Delta\alpha}(z)}{\alpha}. \tag{2.3}$$

Here $\varepsilon(z)$ is the local dielectric constant for the frequency of the light wave, given in terms of $\rho(z)$ approximately by the Clausius–Mossotti relation, ε^L and ε^G are the bulk values, α is the mean polarizability of a molecule, and $\overline{\Delta\alpha}(z)$ is given by

$$\overline{\Delta\alpha}(z) = \Delta\alpha_\parallel \eta_{2,0}(z) + \Delta\alpha_\perp \eta_{2,2}(z)/\sqrt{6} \tag{2.4}$$

where $\Delta\alpha_\parallel \equiv \alpha_{z'z'} - \alpha$ and $\Delta\alpha_\perp \equiv \alpha_{x'x'} - \alpha_{y'y'}$ are molecular polarizability anisotropies, with $\alpha_{x'x'}$, etc principal-axis components†. The local order parameters $\eta_{l,n}(z)$ are defined

† For the definition of the principal axes used, see [20], p 582. Briefly, z' is the twofold axis, and $z'x'$ is the molecular plane.

in (3.10) below. The term (2.3) contains the information about the preferred molecular orientations in the interface. As discussed in section 4, for water this term is found to be several orders of magnitude smaller than the isotropic contribution η_0 and may be difficult to detect experimentally.

2.4. Second-harmonic generation

If the incident beam in figure 2 has frequency ω, the reflected beam also has frequency ω to a good approximation. However, with high-intensity laser sources, one can detect small additional components at frequency $2\omega, 3\omega, \ldots$ [21]; it is the 2ω component, the second-harmonic generation (SHG), which interests us here.

The SHG has its molecular origin in the hyperpolarizability $\boldsymbol{\beta}$ of a molecule. In the presence of an external electric field $\boldsymbol{E}(t) = \boldsymbol{E}_0 \cos \omega t$, the dipole moment $\boldsymbol{\mu}_{\text{ind}}$ induced in a molecule is given by (see, e.g., [20], p 540)

$$\boldsymbol{\mu}_{\text{ind}} = \boldsymbol{\alpha} \cdot \boldsymbol{E} + \tfrac{1}{2}\boldsymbol{\beta} : \boldsymbol{EE} + \ldots \tag{2.5}$$

where the additional terms . . . do not concern us here. In (2.5), $\boldsymbol{\alpha} \cdot \boldsymbol{E}$ is the usual linear response term, with $\boldsymbol{\alpha}$ the polarizability, and $\frac{1}{2}\boldsymbol{\beta} : \boldsymbol{EE}$ is the non-linear response term. If $\boldsymbol{E}$ varies at frequency ω, $\boldsymbol{EE}$ will vary at 2ω, so that SHG arises.

One can relate the nonlinear macroscopic susceptibility $\chi^{(s)}$ to $\boldsymbol{\beta}$ in the same way that one relates the linear susceptibility χ to $\boldsymbol{\alpha}$. To lowest order in $\boldsymbol{\beta}$, neglecting local field effects, one finds [21]

$$\chi^{(s)} = \int_{-\infty}^{\infty} \mathrm{d}z\, \rho(z) \langle \boldsymbol{\beta} \rangle. \tag{2.6}$$

We see from (2.6) that to obtain non-vanishing SHG we require: (i) $\boldsymbol{\beta} \neq 0$, that is molecules such as HCl and H_2O, which lack a centre of inversion: (ii) $\langle \boldsymbol{\beta} \rangle \neq 0$, that is the orientational average must be non-vanishing. In bulk liquid and gas, $\langle \boldsymbol{\beta} \rangle = 0$, so that (2.6) will be sensitive only to the surface molecules, where there are preferred orientations.

For H_2O, as shown in section 4.5, $\langle \boldsymbol{\beta} \rangle$ can be expressed in terms of the following three order parameters $\eta_{l,n}(z)$ defined in (3.10): $\eta_{1,0}$, $\eta_{3,0}$ and $\eta_{3,2}$. The principal-axis components $\beta_{z'z'z'}$, $\beta_{z'x'x'}$, $\beta_{z'y'y'}$ of $\boldsymbol{\beta}$ (see footnote on p F111) are also involved.

Of the four experiments described SHG appears to be the best candidate for studying the alignment of molecules at surfaces. The method is, however, limited to non-centrosymmetric molecules.

3. Theory

The present calculations are based on an extended mean-field theory [3, 11] for non-uniform molecular fluids, which generalizes the density-functional methods used in recent years for studying interfaces of liquid crystals [22, 23] as well as other systems [8, 9]. The particular generalization of these earlier theories is intended to include non-linear (in practice, quadratic) orders of the anisotropic part of the intermolecular pair potential in the free-energy functional. This is motivated by the failure of standard mean-field theory, as well as other approaches that contain only linear orders of the anisotropic potential [6, 7], to account for any interfacial orientational ordering induced by purely multipolar anisotropies. An extended mean-field theory similar to the one considered here was first introduced by Teixeira and Telo da Gama [11] and was applied to a model

fluid with dipole–dipole interactions. The free-energy functional employed in the present work differs slightly from that in [11], as pointed out below. Furthermore, we generalize the anisotropic part of the potential to include dipole–quadrupole and quadrupole–quadrupole couplings, which appear in a more suitable model [24] for the description of water.

A derivation of the extended mean-field theory is described elsewhere [3], and here we shall merely summarize the key points. The theory is based on an intermolecular pair potential of the form

$$V(\mathbf{r}_1\omega_1, \mathbf{r}_2\omega_2) = V_{\text{ref}}(r_{12}) + V_{\text{pert}}(\mathbf{r}_1\omega_1, \mathbf{r}_2\omega_2) \tag{3.1}$$

where $\mathbf{r}_i$ and $\omega_i \equiv (\theta_i, \varphi_i, \chi_i)$ denote the position and Euler angles of molecule i. The isotropic reference potential V_{ref} is assumed to depend only on the intermolecular distance $r_{12} \equiv |\mathbf{r}_2 - \mathbf{r}_1|$. The 'perturbative' part of the interaction is in turn decomposed as

$$V_{\text{pert}}(\mathbf{r}_1\omega_1, \mathbf{r}_2\omega_2) = V_{\text{att}}(r_{12}) + V_{\text{an}}(\mathbf{r}_1\omega_1, \mathbf{r}_2\omega_2). \tag{3.2}$$

In keeping with a 'van der Waals' type of description, V_{ref} is regarded as purely repulsive, and here is taken as a hard-sphere potential with molecular diameter σ. The function V_{att} describes isotropic attractive interactions, while all anisotropic components of the potential are contained in V_{an}.

The theory consists of expressing the grand potential Ω as a functional of the one-particle probability density $\rho(\mathbf{r}, \omega)$,

$$\Omega = \Omega_{\text{ref}} + \Delta\Omega_{\text{MF}} + \Delta\Omega_{\text{EMF}}. \tag{3.3}$$

The first term Ω_{ref} is the total contribution to the grand potential that results from the interaction $V_{\text{ref}}(r_{12})$ alone, albeit in the presence of the full probability density $\rho(\mathbf{r}, \omega)$. Applying an often-used local thermodynamic approximation, we have [3, 11, 22, 23]

$$\Omega_{\text{ref}} = \int \mathrm{d}\mathbf{r}\, f_{\text{ref}}(\rho(\mathbf{r})) + \int \mathrm{d}\mathbf{r}\, \mathrm{d}\omega\, \rho(\mathbf{r}, \omega)\{kT \ln[8\pi^2 \hat{f}(\mathbf{r}, \omega)] - \mu_c\} \tag{3.4}$$

where $f_{\text{ref}}(\rho)$ is the bulk Helmholtz free-energy density of a uniform reference fluid with number density ρ, with μ_c the total chemical potential of the system. The second integral in (3.4) includes the contribution of the orientational entropy, where $\hat{f}(\mathbf{r}, \omega)$ is the normalized orientation distribution function

$$\begin{aligned} \hat{f}(\mathbf{r}, \omega) &= \rho(\mathbf{r}, \omega)/\rho(\mathbf{r}) \\ \rho(\mathbf{r}) &= \int \mathrm{d}\omega\, \rho(\mathbf{r}, \omega). \end{aligned} \tag{3.5}$$

The second term in (3.3), $\Delta\Omega_{\text{MF}}$, describes the mean-field average of the perturbative potential,

$$\Delta\Omega_{\text{MF}} = \tfrac{1}{2} \int \mathrm{d}\mathbf{r}_1\, \mathrm{d}\omega_1\, \mathrm{d}\mathbf{r}_2\, \mathrm{d}\omega_2\, \rho(\mathbf{r}_1, \omega_1) V_{\text{pert}}(12) \rho(\mathbf{r}_2, \omega_2). \tag{3.6}$$

The third term in (3.3), $\Delta\Omega_{\text{EMF}}$, accounts for corrections to the mean-field approximation, and is given here by [3]

$$\begin{aligned} \Delta\Omega_{\text{EMF}} = &-\frac{\beta}{4} \int \mathrm{d}\mathbf{r}_1\, \mathrm{d}\omega_1\, \mathrm{d}\mathbf{r}_2\, \mathrm{d}\omega_2\, \rho(\mathbf{r}_1, \omega_1)[V_{\text{an}}(12)]^2 \rho(\mathbf{r}_2, \omega_2) \\ &-\frac{\beta}{4} \int \mathrm{d}\mathbf{r}_1\, \mathrm{d}\mathbf{r}_2\, \rho(\mathbf{r}_1)\rho(\mathbf{r}_2) \left(\int \mathrm{d}\omega_1\, \mathrm{d}\omega_2\, \hat{f}(\mathbf{r}_1, \omega_1) V_{\text{an}}(12) \hat{f}(\mathbf{r}_2, \omega_2) \right)^2 \\ &+\frac{\beta}{2} \int \mathrm{d}\mathbf{r}_1\, \mathrm{d}\mathbf{r}_2\, \rho(\mathbf{r}_1)\rho(\mathbf{r}_2) \int \mathrm{d}\omega_1\, \hat{f}(\mathbf{r}_1, \omega_1) \left(\int \mathrm{d}\omega_2\, V_{\text{an}}(12) \hat{f}(\mathbf{r}_2, \omega_2) \right) \end{aligned} \tag{3.7}$$

where $\beta \equiv (kT)^{-1}$ is the inverse temperature. This has been derived in [3] from the leading-order correction to mean-field theory in powers of the inverse range of the perturbation V_{pert} [25], formally assuming the latter to the be weak and of long range, and with the additional approximations of keeping only quadratic terms in V_{pert} and replacing reference fluid correlation functions by their high-density limits. Note that (3.7) contains only the anisotropic component $V_{an}(12)$ rather than the full perturbation $V_{pert}(12)$, as it is easy to show that the isotropic component $V_{att}(12)$ cancels from that expression. This differs from the form of the correction term used in [11], which retains only the first line in (3.7) with the full V_{pert} (12) in place of $V_{an}(12)$. In practice we have made one simplification of (3.7), namely to retain only up to quadratic order in the difference of the distribution function from its isotropic limit, $\Delta\hat{f}(r, \omega) \equiv \hat{f}(r, \omega) - 1/8\pi^2$, motivated by the anticipated weakness of interfacial orientational ordering.

The equilibrium probability density $\rho(r, \omega)$ is the solution of the variational condition $\delta\Omega/\delta\rho(r, \omega) = 0$. This leads [3] to coupled integral equations for $\rho(r)$ and $\hat{f}(r, \omega)$ that we shall not write out explicitly here. For the potential components, we have chosen

$$\begin{aligned} V_{att}(r_{12})^6 &= -4\varepsilon(\sigma/r_{12})^6 \qquad r_{12} > \sigma \\ &= 0 \qquad\qquad\qquad r_{12} < \sigma \end{aligned} \tag{3.8}$$

with $V_{an}(12)$ the potential generated by the presence of a point dipole $\boldsymbol{\mu}$ and non-axial point quadrupole $\mathbf{Q}$ at the centre of each molecule,

$$\begin{aligned} V_{an}(12) &= V_{\mu\mu}(12) + V_{\mu Q}(12) + V_{Q\mu}(12) + V_{QQ}(12) \qquad r_{12} > \sigma \\ &= 0 \qquad\qquad\qquad\qquad\qquad\qquad\qquad\qquad r_{12} < \sigma. \end{aligned} \tag{3.9}$$

The potentials (3.8) and (3.9) can be taken equal to zero for $r_{12} < \sigma$ because of the hard-sphere core potential. Explicit expressions for the multipolar interactions $V_{\mu\mu}(12)$, etc, in terms of distance r_{12} and generalized spherical harmonics $D^l_{m_1 n_1}(\omega_i)$ of the molecular orientations, are given in [20]. We assume the molecular symmetry is C_{2v}, as is appropriate for water.

The theory has been applied to a planar interface between coexisting liquid and vapour phases. The probability density is assumed to vary spatially only in the direction z normal to the interface, with positive z on the vapour side as in figure 2. All spatial integrals entering the theory can then be reduced to one-dimensional quadratures along z, involving the number density $\rho(z)$ and several orientational order parameters $\eta_{l,n}(z)$ defined as

$$\begin{aligned} \eta_{l,n}(z) &= \langle D^l_{0n}(\omega)^* \rangle + \langle D^l_{0-n}(\omega)^* \rangle \quad n \neq 0 \\ \eta_{l,0}(z) &= \langle D^l_{00}(\omega)^* \rangle = \langle P_l(\cos\theta) \rangle \end{aligned} \tag{3.10}$$

where P_l is the lth-order Legendre polynomial. Implicit here is the fact that the distribution function $\hat{f}(z, \omega)$ should be independent of the azimuthal orientation of the molecular dipole axis about the z-axis, because of rotational isotropy in the plane of the interface. The relevant Euler angles in ω are then θ and χ, the former denoting the angle between the molecular dipole (or z') and the space-fixed z-axis, and the latter denoting the angle between the molecular symmetry plane (or $x'z'$ plane) and the zz' plane [20]. See figure 3.

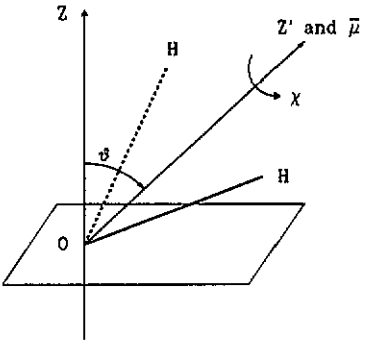

Figure 3. The orientation of a water molecule; z is the space-fixed axis and z' is the body-fixed axis.

The solution of the integral equations for $\rho(z)$ and $\hat{f}(z, \omega)$ is obtained by spherical harmonic and iterative techniques similar to those used in previous work [22, 23]. For given molecular interaction parameters and temperature T, the solution requires specifying the chemical potential μ_c as well as the densities ρ_G and ρ_L of the bulk coexisting vapour and liquid, the latter entering as boundary values for $\rho(z)$ in the limits $z \to \infty$ and $z \to -\infty$, respectively. These are found by applying a double-tangent construction to the bulk Helmholtz free-energy corresponding to this theory, as described in more detail elsewhere [3]. The Carnahan–Starling approximation is used for the reference hard-sphere free-energy density $f_{ref}(\rho)$. Note that, because of the rotational isotropy of the bulk phases, the order parameters $\eta_{l,n}(z)$ vanish in the limits $z \to \pm\infty$.

4. Results and comparison with experimental observables

4.1. Molecular parameters

We have implemented the preceding theory using values of the dipole and quadrupole moments consistent with the charge distribution of the TIP4P model of water [26]. These are listed in table 1, along with our choices for the isotropic interaction parameters ε and σ. The former is equal to the Lennard-Jones strength parameter ε_{LJ} of the TIP4P model [26]. Rather than equating σ with the corresponding Lennard-Jones diameter of the TIP4P model, we have instead varied values of σ to yield a theoretical value for the

Table 1. Values of the molecular potential parameters for water used in this work: μ is the magnitude of the dipole moment and $Q_{\alpha'\alpha'}$ are principal-axis components of the quadrupole moment, with the origin taken at the oxygen atom.

μ (10^{-18} esu)	$Q_{z'z'}$ (10^{-26} esu)	$Q_{x'x'} - Q_{y'y'}$ (10^{-26} esu)	ε (10^{-14} erg)	σ (Å)
2.1773	0.17119	4.29311	1.0777	2.95

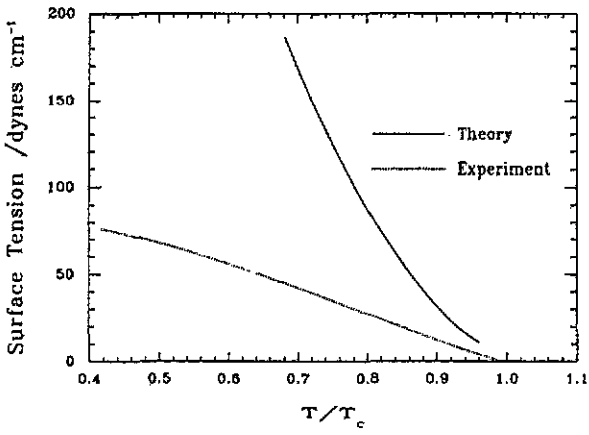

Figure 4. The water interfacial tension γ as a function of T/T_c.

liquid–vapour critical temperature T_c comparable with experimental and simulation values for water [3]. The value quoted in table 1, $\sigma = 2.95$ Å, results in $T_c = 604.97$ K.

It is important to mention that the values of the quadrupole moments listed in table 1 are based on choosing the molecular centre at the site of the oxygen atom in the water molecule. This is consistent with the centre used for the spherically symmetric Lennard-Jones component of the TIP4P model. The significance of this choice of centre is that it yields a positive value for the $Q_{z'z'}$ quadrupole moment. We have shown in detail elsewhere [3] that, in the present theory, the direction of interfacial dipolar alignment is determined by the sign of $Q_{z'z'}$, such that a positive value of the latter results in a preference for surface dipoles to point towards the liquid. This agrees with the earlier work by Stillinger and Ben-Naim [24].

4.2. Interfacial tension and structure

The basic results of the calculations are the interfacial tension γ (given by the excess grand potential per unit area), the density profile $\rho(z)$, the orientational distribution function $\hat{f}(z, \omega)$, and the order parameters $\eta_{l,n}(z)$ derived from $\hat{f}(z, \omega)$ according to (3.10). One drawback of the present theory, which we attribute to its basis in a perturbation expansion in powers of $V_{\text{pert}}(12)$, is that it is limited to fairly high temperatures. In particular, for the present choice of interaction parameters, the interface becomes unstable at temperatures lower than 400 K. Below this temperature, $\rho(z)$ and $\hat{f}(z, \omega)$ develop oscillations which, on iteration, increase in both range and amplitude and appear to grow into the bulk liquid. In addition, the interfacial tension γ begins to decrease with decreasing temperature. These features suggest that the bulk isotropic liquid becomes unstable relative to an ordered, smectic-like phase [3]. Despite this limitation, comparison of our results [3] with those of computer simulations indicates that the theory gives the correct interfacial orientational structure in the temperature regime of its stability.

Figure 4 shows the interfacial tension γ as a function of reduced temperature T/T_c in the high-temperature region, to within a few degrees of the critical point. The divergence of the interfacial width closer to T_c precludes accurate numerical calculations in this limit. The experimental surface tension is also shown (with abscissa scaled in terms of the experimental value, $T_c = 647$ K). The theoretical surface tension is seen to

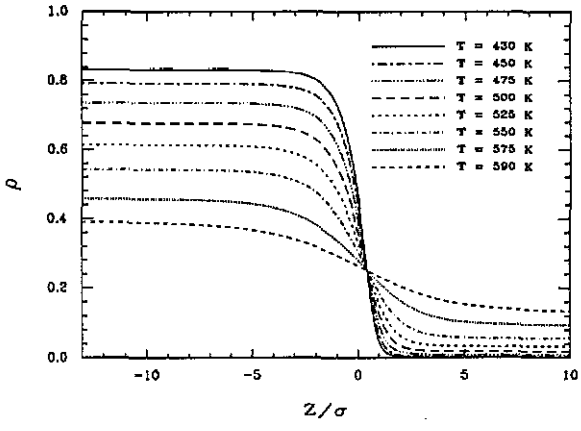

Figure 5. The number density profile of water for various temperatures as a function of z/σ, where σ is the hard-sphere diameter.

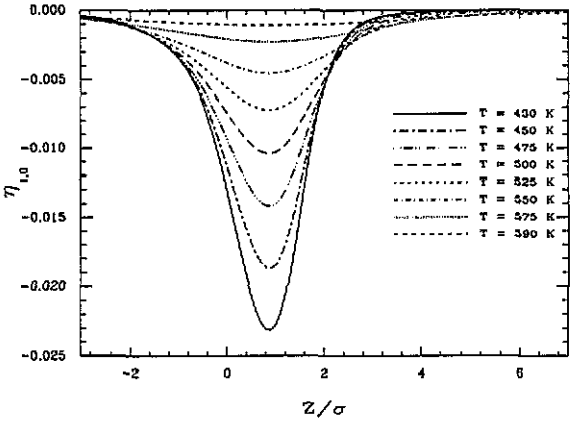

Figure 6. The order parameter $\eta_{1,0}(z)$ for various temperatures.

increase much more rapidly with decreasing temperature compared with the experimental data, related to the inadequacy of the theory at low temperatures. Note that, in the temperature range shown in figure 4, the theoretical curve does not exhibit the inflection point associated with the onset of decreasing surface entropy, which was described in section 2.1.

Curves of the calculated number density $\rho(z)$ at various temperatures in the allowed range of the theory are shown in figure 5. These exhibit the expected broadening of the interfacial width with increasing T/T_c.

For displaying the interfacial orientational structure, we focus here on the order parameters $\eta_{l,n}(z)$. Full details of the distribution function $\hat{f}(z, \omega)$ itself are described in [3]. Figures 6 to 8 show plots of the three lowest-order order parameters $\eta_{1,0}(z)$, $\eta_{2,0}(z)$ and $\eta_{2,2}(z)$, respectively. In all cases the order parameters increase in amplitude with decreasing temperature. The order parameter $\eta_{1,0}(z) = \langle \cos \theta \rangle$ is negative throughout the interface, which is consistent with a weak net alignment of the interfacial dipoles pointing towards the bulk liquid. The order parameter $\eta_{2,0}(z) = \langle P_2(\cos \theta) \rangle$ is negative on the liquid side and positive on the vapour side of the interface, as has been found in several other studies [7–13, 23, 27]. These features indicate a preference for molecules to orient their dipole axes parallel to the interface on the liquid side and perpendicular

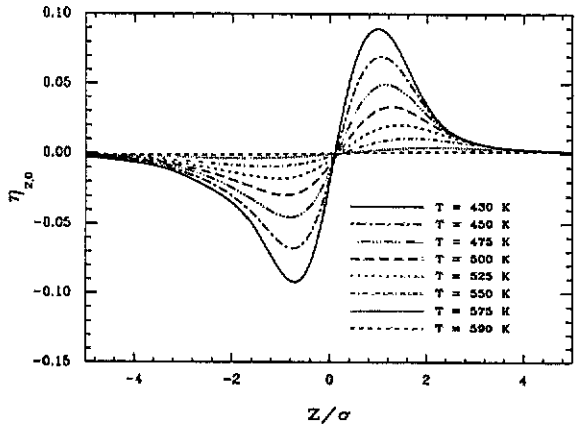

Figure 7. The order parameter $\eta_{2,0}(z)$ for various temperatures.

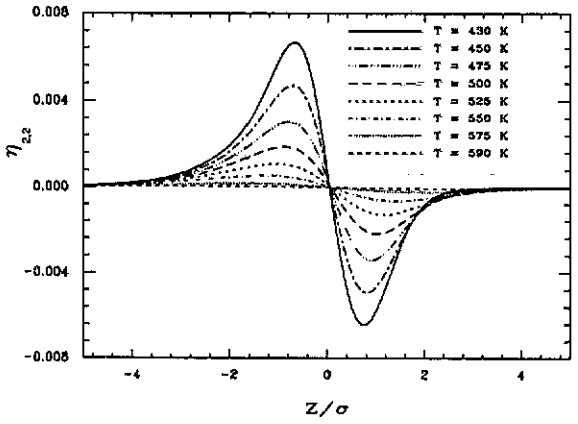

Figure 8. The order parameter $\eta_{2,2}(z)$ for various temperatures.

on the vapour side. The liquid-side tendency generally plays the dominant role in observable interfacial phenomena, owing to the larger number density on this side. On the other hand, the negative value of $\eta_{1,0}$ is mainly the result of a slight asymmetry between the up and down orientations on the vapour side.

The order parameter $\eta_{2,2}(z)$, which, following from (3.10), is explicitly given by $\sqrt{\frac{3}{2}}\langle \sin^2\theta \cos 2\chi \rangle$, exhibits a similar albeit inverted oscillatory behaviour. From its definition this indicates that, on average, the molecular symmetry planes tend to align perpendicular to the interface (i.e. $\chi \approx 0$) on the liquid side and parallel ($\chi \approx 90°$) on the vapour side.

4.3. Surface electric field and potential

We now apply the preceding results to the calculation of the surface potential $\Delta\varphi$. We also consider the macroscopic interfacial electric field, which by symmetry only exhibits a component $E_z(z)$ in the direction normal to the interface. Following the analysis of

Wilson *et al* [19] the following expression is a multipole representation of the electric field for a system of electrically neutral molecules

$$E_z(z) = -4\pi\left(P_z(z) - \frac{1}{2}\frac{\mathrm{d}}{\mathrm{d}z}\Theta_{zz}(z) + \ldots\right) \tag{4.1}$$

where $P_z(z)$ is the z-component of the dipole density and $\Theta_{zz}(z)$ is the zz-component of the quadrupole density. The electrostatic potential $\varphi(z)$ at position z, relative to the potential $\varphi(\infty)$ in the bulk vapour phase, is then obtained from the integral of the field,

$$\Delta\varphi(z) \equiv \varphi(z) - \varphi(\infty) = \int_z^\infty \mathrm{d}z'\, E_z(z')$$

$$= -4\pi\int_z^\infty \mathrm{d}z'\, P_z(z') - 2\pi[\Theta_{zz}(z) - \Theta_{zz}(\infty)] + \ldots. \tag{4.2}$$

The total potential difference between the bulk phases follows on taking the limit $z \to -\infty$ in (4.2),

$$\Delta\varphi = -4\pi\int_{-\infty}^\infty \mathrm{d}z'\, P_z(z') - 2\pi[\Theta_{zz}(-\infty) - \Theta_{xz}(\infty)]. \tag{4.3}$$

In contrast to (4.1) and (4.2) the truncation at the quadrupolar level in (4.3) is exact since higher multipole terms involve z-derivatives that vanish in the bulk phases.

The mean polarization $P_z(z)$ is related to the number density and the order parameter $\eta_{1,0}(z) = \langle\cos\theta\rangle$ by

$$P_z(z) = \mu\rho(z)\eta_{1,0}(z). \tag{4.4}$$

In an analogous way, $\Theta_{zz}(z)$ is related to the angular average of the molecular quadrupole moment. For arbitrary Cartesian components α, β, we have

$$\Theta_{\alpha\beta}(z) = \rho(z)\left\langle\sum_i q_i r_{i\alpha} r_{i\beta}\right\rangle \equiv \rho(z)\langle\Theta_{\alpha\beta}(\omega)\rangle \tag{4.5}$$

where $r_{i\alpha}$ is the α-component of the position of the partial charge q_i relative to an arbitrarily chosen centre. It is to be noted that the tensor $\Theta_{\alpha\beta}(\omega)$ defined in (4.5) contains a non-vanishing trace and thus differs from the conventional quadrupole moment $Q_{\alpha\beta}(\omega)$, to which it is related by

$$Q_{\alpha\beta}(\omega) = \tfrac{3}{2}[\Theta_{\alpha\beta}(\omega) - \Theta\delta_{\alpha\beta}] \tag{4.6}$$

where $\Theta = \mathrm{Tr}\,\boldsymbol{\Theta}/3$. Although the occurrence of $\Theta_{\alpha\beta}$ rather than $Q_{\alpha\beta}$ in these expressions may seem unusual, this is related to an important condition, namely that the physical quantities $E_z(z)$ and $\Delta\varphi(z)$ are in fact independent of the choice of molecular origin, which is arbitrary. (This exact condition strictly requires that the multipole series in (4.1) and (4.2) be carried to all orders.) As discussed in [19], this condition is violated if only the dipole density term is retained in (4.1) to (4.3), which argues against the latter method for evaluating interfacial electrostatic properties [14, 16].

From (4.5) and (4.6), and using the C_{2v} symmetry of the water molecule (taking the origin on the symmetry axis), it is straightforward to show that

$$\Theta_{zz}(z) = \rho(z)[\Theta + \tfrac{3}{2}Q_{z'z'}\eta_{2,0}(z) + \tfrac{1}{2}\sqrt{\tfrac{3}{2}}(Q_{x'x'} - Q_{y'y'})\eta_{2,2}(z)]. \tag{4.7}$$

For the TIP4P model [26], we find that $\Theta = 1.488 \times 10^{-26}$ esu. Noting the magnitudes of

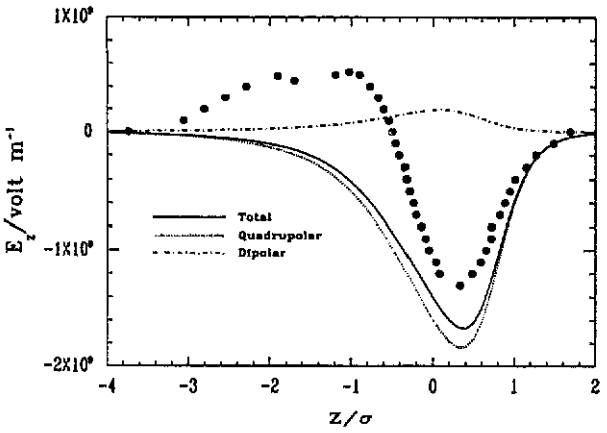

Figure 9. The total electric field $E_z(z)$ and the separate dipolar and quadrupolar contribution to $E_z(z)$ at $T = 430$ K. The points are the simulation results from [5] at $T = 325$ K.

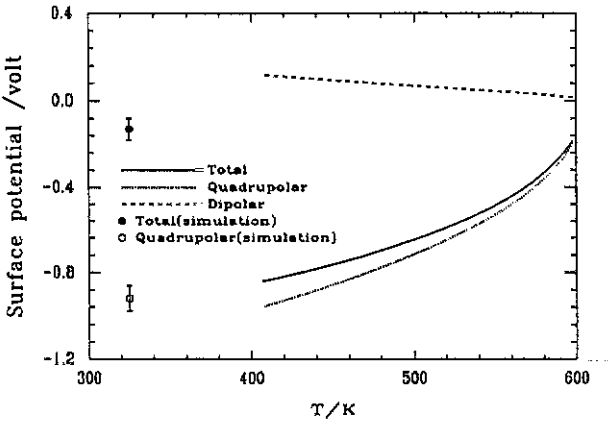

Figure 10. The surface potential $\Delta\varphi$, as well as the separate dipolar and quadrupolar contributions to $\Delta\varphi$ as a function of temperature. The simulation data are from [5] and [19].

$\eta_{2,0}$ and $\eta_{2,2}$ from figures 7 and 8, one sees that the second and third terms in (4.7) contribute at most 1% to the value of $\Theta_{zz}(z)$ and hence are essentially negligible. Thus $\Theta_{zz}(z) \simeq \rho(z)\Theta$ for all z. This is of course exact in the bulk limits, and substitution into (4.3) then gives the result given earlier in (2.1).

The electric field calculated from (4.1) at $T = 430$ K is plotted in figure 9, along with the separate contributions from P_z and $d\Theta_{zz}/dz$. It is clear that the dominant contribution comes from the quadrupole term, which is essentially proportional to the density gradient $d\rho/dz$ and thus has no direct connection to surface orientation ordering. The simulation results for E_z from [5] are shown for comparison. The qualitative agreement between the magnitudes of the theoretical and simulation results must be viewed as quite fortuitous, however, since they pertain to quite different temperatures, the simulations being at $T = 325$ K. A noticeable difference between the data is the occurrence of a zero in E_z and positive values of the latter at negative (liquid side) distances z according to the simulations, which are absent from the present theoretical results. This suggests there is a more substantial dipolar contribution from P_z at the lower temperature of the simulation study.

The total surface potential $\Delta\varphi$ according to the present theory is shown in figure 10 as a function of T. Here again the separate dipolar and quadrupolar contributions are

presented, once more indicating the dominance of the latter, which in this case depends only on the difference in bulk densities and the value of Θ. At $T = 430$ K, the dipolar and quadrupolar contributions are approximately 0.1 V and −0.9 V, respectively. A rough extrapolation to lower temperature indicates that the dipolar contribution is much weaker than that given by the simulations of Wilson *et al* [5, 19], while the magnitude of the quadrupolar term is about 20% larger, the latter because of the larger density difference $\rho_L - \rho_G$ predicted by the present theory. As discussed in [5], the negative sign of the total calculated value of $\Delta\varphi$ disagrees with that inferred from recent experiments, which would be consistent with the dipolar contribution alone. Since the methods for measuring $\Delta\varphi$ are indirect, it appears that the surface potential is anappropriate for comparing theory and experiment, and that further studies of interfacial electrostatics should examine more directly measureable quantities.

4.4. Ellipsometry

The quantity usually considered in ellipsometry is the coefficient of ellipticity $\bar{\rho}$, given by [14, 28]

$$\bar{\rho} = \frac{\pi}{\lambda}\frac{(\varepsilon^G + \varepsilon^L)^{1/2}}{(\varepsilon^G - \varepsilon^L)}\eta \tag{4.8}$$

where λ is the wavelength of the light beam used in the experiment, and

$$\eta = \int_{-\infty}^{\infty} dz \left(\varepsilon_\parallel(z) + \frac{\varepsilon^G\varepsilon^L}{\varepsilon_\perp(z)} - \varepsilon^G - \varepsilon^L\right). \tag{4.9}$$

Here $\varepsilon_\parallel(z) = \varepsilon_{xx}(z)$ and $\varepsilon_\perp(z) = \varepsilon_{zz}(z)$ are components of the inhomogeneous dielectric tensor parallel and perpendicular to the interface, respectively. Following Matsumoto and Kataoka [14] and assuming the Clausius–Mossotti formula, we relate the components of the dielectric tensor to the number density and the corresponding components of the mean polarizability tensor by

$$\varepsilon_{\gamma\gamma}(z) = (1 + \tfrac{8}{3}\pi\rho(z)\langle\alpha_{\gamma\gamma}\rangle)/(1 - \tfrac{4}{3}\pi\rho(z)\langle\alpha_{\gamma\gamma}\rangle). \tag{4.10}$$

Here $\langle\alpha_{\gamma\gamma}\rangle$ denotes the average over angles, weighted by $\hat{f}(z, \omega)$, of the space-fixed $\gamma\gamma$ component of single-molecular polarizability tensor. Rewriting equation (23) of [14], we have

$$\begin{aligned}\langle\alpha_{xx}\rangle &= \alpha - \overline{\Delta\alpha}(z)/2\\ \langle\alpha_{zz}\rangle &= \alpha + \overline{\Delta\alpha}(z)\end{aligned} \tag{4.11}$$

where $\overline{\Delta\alpha}(z)$ is defined in (2.4). Since we find (see below) that $|\overline{\Delta\alpha}(z)| \ll \alpha$, an accurate approximation to η is obtained by linearizing (4.9) and (4.10) in $\overline{\Delta\alpha}(z)/\alpha$, which leads to $\eta = \eta_0 + \Delta\eta$ with the latter quantities given by (2.2) and (2.3). As usual, the integral for $\Delta\eta$ will be dominated by contributions from the liquid side of the interface, since the factor $\varepsilon(z) - 1 \approx \varepsilon^G - 1$ is very small on the vapour side.

As in [14], we use the values of Murphy [29] for the polarizability components of water. These values yield

$$\alpha = 1.470 \times 10^{-24}\ \text{cm}^3 \qquad \Delta\alpha_\parallel = -0.00233 \times 10^{-24}\ \text{cm}^3$$
$$\Delta\alpha_\perp = 0.113 \times 10^{-24}\ \text{cm}^3. \tag{4.12}$$

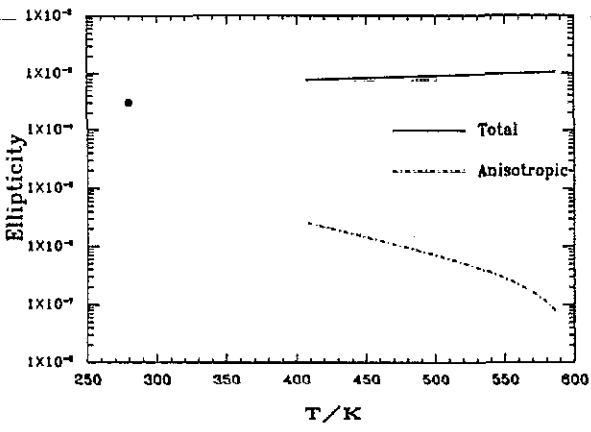

Figure 11. The total ellipticity coefficient $\bar{\rho}$ and the contribution to $\bar{\rho}$ from $\Delta\eta$ as a function of temperature. The point gives the experimental result from [30].

Noting from figures 7 and 8 that, on the liquid side of the interface, $\eta_{2,0}$ is negative with a maximum magnitude $|\eta_{2,0}| \simeq 0.1$, while $\eta_{2,2}$ is positive and has a maximum magnitude $\eta_{2,2} \simeq 0.01$, one sees using (4.12) that both terms in (2.4) give *positive* contributions to $\Delta\alpha(z)/\alpha$, with a total magnitude of about 5×10^{-4}. (Note, however, that the value of $\Delta\alpha_{\parallel}$ is only marginally negative, and a slight shift in the values of the polarizability components could result in the opposite sign for $\Delta\alpha(z)$.) It follows from (2.3) that $\Delta\eta$ is negative, which is the same sign as η_0 but roughly three orders of magnitude smaller. This is shown in figure 11, where we separately plot the total ellipticity coefficient $\bar{\rho}$ and the contribution to $\bar{\rho}$ from $\Delta\eta$. Note that the total value of $\bar{\rho}$ increases slowly with increasing temperature, and this is attributed to broadening of the interface that affects the isotropic component η_0, while the anisotropic component decreases with temperature because of weakening of the orientational order. A smooth extrapolation of the curve for $\bar{\rho}$ to lower temperature yields good agreement with both experimental results [30] and the simulation results of Matsumoto and Kataoka [14].

The very small magnitude of $\Delta\eta$ compared with η_0 is consistent with the findings of Matsumoto and Kataoka [14], but disagrees with the speculations by Beaglehole [30]. Our result that $\Delta\eta$ is negative appears to disagree with that of Matsumoto and Kataoka [14]. Since we have used the same values for the polarizability as in [14], and both of our works agree in predicting a predominantly parallel dipolar alignment on the liquid size ($z < 0$), we conclude that the difference arises from different results for the sign of $\eta_{2,2}$, which as discussed earlier is mainly sensitive to the distribution of the rotation angle χ.

4.5. Second-harmonic generation

The final observable considered here is the nonlinear macroscopic susceptibility $\boldsymbol{\chi}^{(s)}$ associated with SHG. As described in section 2.4, $\boldsymbol{\chi}^{(s)}$ is related to the average over angles $\langle\boldsymbol{\beta}\rangle$ of the molecular hyperpolarizability tensor. This average over angles can be performed by using the relation between space-fixed (α, β, γ) and body-fixed (α', β', γ') components of the third-rank tensor $\boldsymbol{\beta}$,

$$\beta_{\alpha\beta\gamma}(\omega) = D_{\alpha\alpha'}(\omega)D_{\beta\beta'}(\omega)D_{\gamma\gamma'}(\omega)\beta_{\alpha'\beta'\gamma'} \tag{4.13}$$

where the summation convention is implied. Here $D_{\alpha\alpha'}(\omega) \equiv \cos\theta_{\alpha\alpha'}$ denotes the direction cosine between the space-fixed, α, and body-fixed, α', axes. For a molecule with C_{2v} symmetry, the non-vanishing body-fixed components of $\boldsymbol{\beta}$ are

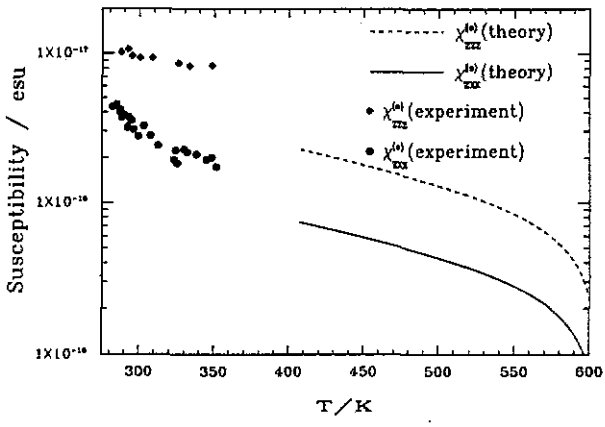

Figure 12. The susceptibility $\chi^{(s)}$ as a function of temperature. Experimental data are from [31], as described in the text.

$$\begin{aligned}
\beta_{z'z'z'} &\equiv \beta_0 \\
\beta_{z'x'x'} &= \beta_{x'z'x'} = \beta_{x'x'z'} \equiv \beta_1 \\
\beta_{z'y'y'} &= \beta_{y'z'y'} = \beta_{y'y'z'} \equiv \beta_2
\end{aligned} \tag{4.14}$$

where we have assumed the static limit, that is we neglect dispersion effects. A straightforward calculation, taking into account the azimuthal symmetry of the interface, then leads to the following results for the non-zero components of $\langle\boldsymbol{\beta}\rangle$:

$$\begin{aligned}
\langle\beta_{zxx}\rangle = \langle\beta_{zyy}\rangle \qquad & \textit{(and permutations)} \\
&= \tfrac{1}{8}\beta_0(\eta_{1,0} - \eta_{3,0}) + \tfrac{1}{20}\beta_1(4\eta_{1,0} + 6\eta_{3,0} - \sqrt{30}\eta_{3,2}) \\
&\quad + \tfrac{1}{20}\beta_2(4\eta_{1,0} + 6\eta_{3,0} + \sqrt{30}\eta_{3,2}) \qquad (4.15a)
\end{aligned}$$

$$\begin{aligned}
\langle\beta_{zzz}\rangle = \tfrac{1}{8}(3\eta_{1,0} + 2\eta_{3,0}) + \tfrac{3}{10}\beta_1(2\eta_{1,0} - 2\eta_{3,0} + \sqrt{\tfrac{10}{3}}\,\eta_{3,2}) \\
+ \tfrac{3}{10}\beta_2(2\eta_{1,0} - 2\eta_{3,0} - \sqrt{\tfrac{10}{3}}\,\eta_{3,2}) \qquad (4.15b)
\end{aligned}$$

where $\eta_{3,2}(z) = \sqrt{\frac{15}{2}}\langle\sin^2\theta\cos\theta\cos 2\chi\rangle$. The relations in (4.15) satisfy the sum rule (generalizing that mentioned in [31])

$$\langle\beta_{zzz}\rangle + 2\langle\beta_{zxx}\rangle = (\beta_0 + \beta_1 + \beta_2)\eta_{1,0}. \tag{4.16}$$

Note that the components of $\langle\boldsymbol{\beta}\rangle$ are non-zero only in the interfacial region, since the order parameters vanish in the bulk phases. The corresponding components $\chi^{(s)}_{zxx}$ and $\chi^{(s)}_{zzz}$ of the susceptibility are then obtained by integrating across the interface according to (2.6).

The results of the present theory for the susceptibility components as functions of temperature are given in figure 12. For values of the molecular hyperpolarizability, we have extracted the best estimates contained in the recent work by Maroulis [33], which are $\beta_0 = -14.44$, $\beta_1 = -9.95$ and $\beta_2 = -5.61$, in atomic units (au). The susceptibilities are positive and decrease monotonically with temperature. The positive sign is a result of the product of negative β with negative values of the order parameters in (4.15), which are dominated by $\eta_{1,0}(z)$ (see figure 6). In addition, $\chi^{(s)}_{zzz} > \chi^{(s)}_{zxx}$, consistent with (4.15) and dominance by the order parameter $\eta_{1,0}$.

Comparison of our results for $\chi^{(s)}_{zxx}$ and $\chi^{(s)}_{zzz}$ with the recent experimental data of Goh *et al* [31] is problematic, since our calculations are restricted to high temperatures, $T > 400$ K, and the measurements of [31] did not provide absolute values of the susceptibilities. Two other factors complicate the comparison of theory and experiment. The first is the discovery in [31] of a significant difference between the susceptibilities $\chi^{(s)}_{zxx}$ and $\chi^{(s)}_{xzx}$, which should be equal in the static limit under the dipole approximation considered in this work (see (2.5)). While frequency-dependent corrections produce differences $\beta_{x'z'x'} = \beta_{x'x'z'} \neq \beta_{z'x'x'}$ and $\beta_{y'z'y'} = \beta_{y'y'z'} \neq \beta_{z'y'y'}$ in the molecular hyperpolarizabilities that could lead to such differences between the macroscopic susceptibility components, these effects are not expected [32] to be significant at optical frequencies in the case of water. Thus Goh *et al* [31, 32] attributed the difference between $\chi^{(s)}_{xzx}$ and $\chi^{(s)}_{zxx}$ to quadrupolar contributions to the measured SHG signals. The relative importance of the latter effects remains subject to some controversy [34], so we defer analysis of this possibility to future work. The other caveat is that, in ref. [31], it was deduced that the sign of the measured susceptibilities for water is actually *negative*. Goh *et al* interpreted this finding to be consistent with a negative value of $\eta_{1,0}$ by taking positive rather than negative signs for the hyperpolarizabilities, as suggested by earlier measurements of electric-field-induced SHG in bulk water. On the other hand, an earlier measurement [35] of the susceptibilities for a pure water surface yielded a positive value, $\chi^{(s)}_{xzx} = 8.15 \times 10^{-18}$ esu. We have used the latter value (assuming the measurements in [35] were done at room temperature, $T = 295$ K) to provide an absolute scale for the data of Goh *et al* [31], and have plotted these data in figure 12. These are seen to be roughly consistent with extrapolation of our results to lower temperature.

5. Concluding remarks

From our high-temperature extended mean-field theory, together with an isotropic plus point multipole model for the water–water intermolecular potential, we predict the following preferred molecular orientations at the liquid/vapour interface:

(i) the most probable dipole alignment is parallel to the interface on the liquid side, and perpendicular on the vapour side;

(ii) the dipole-down (i.e. protons towards the liquid side) orientation is slightly preferred over the dipole-up orientation;

(iii) the molecular plane tends to align perpendicular to the interface on the liquid side, and parallel on the vapour side.

Of the four experiments discussed, in the case of water, SHG appears to be the best candidate for probing experimentally the preferred molecular orientations at the surface. There are, however, some remaining difficulties to be overcome, both theoretical and experimental, before unambiguous information about the preferred orientations can be extracted from experiment.

Acknowledgments

It is a pleasure to dedicate this paper to Professor Peter Egelstaff on the occasion of his 65th birthday. The authors gratefully acknowledge financial support from the Natural Sciences and Engineering Research Council, Canada.

References

[1] Braslau A, Pershan P S, Swislow G, Ocko B M and Als-Nielson J 1988 *Phys. Rev.* A **38** 2457
[2] Rowlinson J S and Widom B 1982 *Molecular Theory of Capillarity* (Oxford: Clarendon)
[3] Yang B, Sullivan D E, Tjipto-Margo B and Gray C G 1991 *Mol. Phys.* submitted
[4] Wilson M A, Pohorille A and Pratt L R 1987 *J. Phys. Chem.* **91** 4873
[5] Wilson M A, Pohorille A and Pratt L R 1988 *J. Chem. Phys.* **88** 3281
[6] Haile J M, Gubbins K E and Gray C G 1976 *J. Chem. Phys.* **64** 1852
[7] Thompson S M, Gubbins K E and Haile J M 1981 *J. Chem. Phys.* **75** 1325
[8] Tarazona P and Navascués G 1982 *Mol. Phys.* **47** 145
[9] Chacón E, Tarazona P and Navascués G 1983 *J. Chem. Phys.* **79** 4426
[10] Eggebrecht J, Gubbins K E and Thompson S M 1987 *J. Chem. Phys.* **86** 2286
[11] Teixeira P I and Telo da Gama M M 1991 *J. Phys.: Condens. Matter* **3** 111
[12] Thompson S M and Gubbins K E 1981 *J. Chem. Phys.* **74** 6467
[13] Eggebrecht J, Thompson S M and Gubbins K E 1987 *J. Chem. Phys.* **86** 2299
[14] Matsumoto M and Kataoka Y 1988 *J. Chem. Phys.* **88** 3233
[15] Townsend R M and Rice S A 1991 *J. Chem. Phys.* **94** 2207
[16] Matsumoto M and Kataoka Y 1989 *J. Chem. Phys.* **90** 2390
[17] Sprow F B and Prausnitz J M 1966 *Trans. Faraday Soc.* **62** 1097
[18] Floriano M A and Angell C A 1990 *J. Phys. Chem.* **94** 4199 and references therein
[19] Wilson M A, Pohorille A and Pratt L R 1989 *J. Chem. Phys.* **90** 5211
[20] Gray C G and Gubbins K E 1984 *Theory of Molecular Fluids* (Oxford: Clarendon)
[21] Shen Y R 1984 *The Principles of Nonlinear Optics* (New York: Wiley)
[22] Telo da Gama M M 1984 *Mol. Phys.* **52** 585, 611
[23] Tjipto-Margo B, Sen A K, Mederos L and Sullivan D E 1989 *Mol. Phys.* **67** 601
[24] Stillinger F H and Ben-Naim A 1967 *J. Chem. Phys.* **47** 4431
[25] Sullivan D E 1982 *Phys. Rev.* A **25** 1669
[26] Jorgensen W L, Chandrasekhar J, Madura J D, Impey R W and Klein M L 1983 *J. Chem. Phys.* **79** 926
[27] Sluckin T J 1981 *Mol. Phys.* **43** 817
[28] Lekner J 1983 *Mol. Phys.* **49** 1385
[29] Murphy W F 1977 *J. Chem. Phys.* **67** 5877
[30] Beaglehole D 1983 *J. Physique Coll.* C10 **44** 147
[31] Goh M C, Hicks J M, Kemnitz K, Pinto G R, Bhattacharyya K, Eisenthal K B and Heinz T F 1988 *J. Phys. Chem.* **92** 5074
[32] Goh M C and Eisenthal K B 1989 *Chem. Phys. Lett.* **157** 101
[33] Maroulis G 1991 *J. Chem. Phys.* **94** 1182
[34] Andrews D L and Blake N P 1988 *Phys. Rev.* A **38** 3113
Zhu X D and Shen Y R 1990 *Phys. Rev.* A **41** 4549
Heinz T F and di Vincenzo D P 1990 *Phys. Rev.* A **42** 6249
[35] Wang C C 1969 *Phys. Rev.* **178** 1457